

Monitoring surface resonances on $\text{Co}_2\text{MnSi}(100)$ by spin-resolved photoelectron spectroscopy

J. Braun¹, M. Jourdan², A. Kronenberg², S. Chadov³, B. Balke⁴, M. Kolbe², A. Gloskovskii⁵,
H. J. Elmers², G. Schönhense², C. Felser^{3,4}, M. Kläui², H. Ebert¹ and J. Minár^{1,6}

¹*Department Chemie, Ludwig-Maximilians-Universität München, 81377 München, Germany*

²*Institut für Physik, Johannes-Gutenberg-Universität Mainz, Staudingerweg 7, 55128 Mainz, Germany*

³*Max-Planck-Institut für Chemische Physik fester Stoffe, 01187 Dresden, Germany*

⁴*Institut für Anorganische und Analytische Chemie,*

Johannes-Gutenberg-Universität Mainz, Staudingerweg 9, 55128 Mainz, Germany

⁵*Deutsches-Elektronen-Synchrotron DESY, 22603 Hamburg, Germany*

⁶*New Technologies - Research Center, University of West Bohemia, Univerzitni 8, 306 14 Pilsen, Czech Republic*

The magnitude of the spin polarization at the Fermi level of ferromagnetic materials at room temperature is a key property for spintronics. Investigating the Heusler compound Co_2MnSi a value of 93% for the spin polarization has been observed at room temperature, where the high spin polarization is related to a stable surface resonance in the majority band extending deep into the bulk. In particular, we identified in our spectroscopical analysis that this surface resonance is embedded in the bulk continuum with a strong coupling to the majority bulk states. The resonance behaves very bulk-like, as it extends over the first six atomic layers of the corresponding (001)-surface. Our study includes experimental investigations, where the bulk electronic structure as well as surface-related features have been investigated using spin-resolved photoelectron spectroscopy (SR-UPS) and for a larger probing depth spin-integrated high energy x-ray photoemission spectroscopy (HAXPES). The results are interpreted in comparison with first-principles band structure and photoemission calculations which consider all relativistic, surface and high-energy effects properly.

I. INTRODUCTION

For many spintronics applications it is not the bulk, but the surface or interface electronic structure at the Fermi energy given by the difference of the normalized total number of spin up and spin down electrons of the involved materials, which is relevant for applications. However, theoretical predictions for this sample region are much more demanding compared with calculations of bulk properties. A key property for spintronics is the spin polarization at the Fermi level. Concerning surface and interface states it is necessary to distinguish between materials with a finite total spin polarization at the Fermi energy and materials with zero total but momentum dependent spin polarization, which is nonzero for specific k values. Examples for the second class of materials are topological insulators like Bi_2Se_3 ¹, but also simple materials like Bismuth² and Tungsten³. However, the first class of materials, i.e. with a nonzero total spin polarization, can be realized by ferro- or ferrimagnetic materials only. Accordingly, in the following the term spin polarization is always used for the total spin polarization at the Fermi energy. By surface sensitive spin and angular-resolved photoemission spectroscopy (SR-ARPES) values of the spin polarization close to 100% at room temperature were observed for metastable CrO_2 ⁴ and for Fe_3O_4 ⁵, but no corresponding state-of-the-art photoemission calculation and no discussion of possible surface states exists up to now. Furthermore, these materials did not allow for large spin transport effects and are not compatible with other materials relevant for applications. For these reasons intermetallic Heusler compounds⁶ with their predicted half-metallic properties⁷ moved into the focus of

interest⁸⁻¹³. In addition to being interesting for applications, intermetallic Heusler materials represent a test for modern electronic structure calculations for materials with electronic correlations of moderate strength¹⁴⁻¹⁷. In fact, by means of various band structure methods many Heusler compounds have been predicted to be 100% spin-polarized in the bulk. However, the first direct observation of a huge surface spin polarization in any Heusler compound by photoemission spectroscopy was possible only very recently¹⁸. In our preliminary work we identified a 93% polarized surface resonance investigating the Heusler compound Co_2MnSi at room temperature. This represents the first example for such a resonance in any ferromagnetic metal. Within this work we investigate in more detail the occupied as well as the unoccupied electronic structure of Co_2MnSi . Furthermore, we compare our spectroscopical analysis to corresponding experimental data, with special emphasis on surface-related features of the electronic structure.

II. THEORETICAL AND EXPERIMENTAL DETAILS

A. Theoretical and computational details

Experimentally, the interesting valence band region around the Fermi energy is accessible by means of ultraviolet photoemission spectroscopy (PES)¹⁹ and inverse photoemission spectroscopy (IPE)²⁰. From the theoretical point of view the most successful theoretical approach to deal with photoemission is the so-called one-step model as originally proposed by Pendry and co-

workers^{21–23}. A review on the various developments and refinements²⁴ of the approach can be found in Ref. 25. As the most recent development our spectroscopic analysis is based on the fully relativistic one-step model, in its spin-density matrix formulation. This approach allows describing properly the complete spin-polarization vector of the photo current. The corresponding spin-density matrix of the photocurrent is defined by the following equation²⁶:

$$\bar{\rho}_{ss'}^{\text{PES}}(\mathbf{k}_{||}, \epsilon_f) = \langle s, \epsilon_f, \mathbf{k}_{||} | G_2^+ \Delta G_1^+ \Delta^\dagger G_2^- | \epsilon_f, \mathbf{k}_{||}, s' \rangle . \quad (1)$$

It follows then for the spin-density matrix ρ :

$$\rho_{ss'}^{\text{PES}}(\mathbf{k}_{||}, \epsilon_f) = \frac{1}{2i} (\bar{\rho}_{ss'}^{\text{PES}}(\mathbf{k}_{||}, \epsilon_f) - \bar{\rho}_{s's}^{\text{PES}}(\mathbf{k}_{||}, \epsilon_f)) . \quad (2)$$

The intensity of the photocurrent results in:

$$I^{\text{PES}}(\mathbf{k}_{||}, \epsilon_f) = Sp (\rho_{ss'}^{\text{PES}}(\mathbf{k}_{||}, \epsilon_f)) , \quad (3)$$

and the corresponding spin-polarization vector is given by:

$$\mathbf{P} = \frac{1}{I} Sp (\boldsymbol{\sigma} \cdot \rho) , \quad (4)$$

where $\boldsymbol{\sigma}$ denotes the vector of the three Pauli spin matrices. Finally, the spin-projected photocurrent is obtained from the following equation:

$$I_{\mathbf{n}}^{\pm \text{PES}} = \frac{1}{2} (1 \pm \mathbf{n} \cdot \mathbf{P}) I^{\text{PES}} . \quad (5)$$

The spin polarization is calculated with respect to the vector \mathbf{n} . This, for example, allows the complete calculation of all three components of the spin-polarization vector for each pair of (k_x, k_y) values which define the coordinate system for momentum images. Within this formalism I^{PES} denotes the elastic part of the photocurrent. Vertex renormalizations are neglected. This excludes inelastic energy losses and corresponding quantum-mechanical interference terms^{22,27,28}. Furthermore, the interaction of the outgoing photoelectron with the rest system is not accounted for, which means that the so-called sudden approximation has been applied. This approximation is expected to be justified for not too small photon energies. The initial and final states are constructed within spin-polarized low-energy electron diffraction (SPLEED) theory where the final state is represented by a so-called time-reversed SPLEED state^{25,29}. Many-body effects are included phenomenologically in the final-state calculation, using a parameterized, weakly energy-dependent and complex inner potential as in Ref. 21. This generalized inner potential accounts for inelastic corrections to the elastic photocurrent²⁷ as well as the actual (real) inner potential, which serves as a reference energy inside the solid with respect to the vacuum level³⁰. Due to the finite imaginary part, the inelastic mean free path (IMFP) is accounted for and thus the amplitude of the high-energy

photoelectron state can be neglected beyond a certain distance from the surface.

The self-consistent electronic structure calculations were performed within the ab-initio framework of spin-density functional theory, in a fully relativistic mode by solving the corresponding Dirac equation. For the exchange and correlation potential the Perdew-Burke-Enzerhof parametrization was used³¹. To account for electronic correlations beyond the local spin-density approximation (LSDA) we employed a self-consistent combination of the LSDA and the dynamical mean field theory. This computational LSDA+DMFT scheme, self-consistent in both the self-energy calculation and the charge-density calculation is implemented within the relativistic SPR-KKR formalism^{32–35}. The effective DMFT impurity problem was solved through the spin polarized T-matrix fluctuation-exchange (SPTF) solver³⁶, working on a Matsubara energy grid corresponding to a temperature of 400 K. The SPTF solver is accurate for moderately correlated systems as it was shown in several successful applications for various materials³². Simultaneous convergence of the electronic charge-density and the self-energy had been achieved by use of 4096 Matsubara frequencies. The double counting was corrected using the fully localised limit (FLL) scheme (for details concerning DC corrections within KKR calculations see³²). The FLL was successfully applied to Co₂MnSi recently within LSDA+U calculations³⁷, where we used the fully rotationally invariant U-matrix with U-parameters $U_{\text{Mn}}=3.0$ eV and $U_{\text{Co}}=1.5$ eV for Mn and Co. The exchange parameter J was chosen to 0.9 eV for both Mn and Co.

Additionally, for the photoemission calculations, we account for the surface barrier by use of a Rundgren-Malmström-type surface potential⁴², which can be easily included into the formalism as an additional layer. This procedure allows for the correct description of its asymptotic behavior. As this surface barrier represents a z-dependent potential, a surface contribution as part of the total photocurrent results, which accounts explicitly for the energetics and dispersion of all surface features. Furthermore, the relative intensities of surface-related spectral distributions are quantitatively accounted for by calculating the corresponding matrix elements in the surface region. This procedure is described in detail, for example, in Refs. 43,44. Also, energy and momentum conservation are naturally included in the formalism^{25,45}. To take care of impurity scattering, a small constant imaginary value of $V_{i1} = 0.05$ eV was used for the initial state, this way describing the finite life-time of the initial state. Life-time effects in the final state are accounted for by the imaginary part of the inner potential (see above). A constant imaginary value of $V_{i2} = 1.5$ eV has been chosen again in a phenomenological way for excitation energies in the ARPES regime. According to the experimental setup the spectroscopic calculations were performed for linearly p-polarized light.

B. Experimental details

The high reactivity of Heusler materials makes photoemission spectroscopy (PES), the most powerful method for investigations of the electronic band structure of solids, challenging. Sample degradation is a major problem and often results in missing Fermi edges in the photoemission spectra and unexpectedly small experimentally obtained spin polarizations, such as 12% for the predicted half-metal Co_2MnSi ⁴⁶. Sputter cleaning of the samples prior to PES yields slightly increased spin polarization values, for instance 20% for $\text{Co}_2\text{Cr}_{0.6}\text{Fe}_{0.4}\text{Al}$ ⁴⁷. However, in these and many other cases neither the observed spin polarization nor the overall energy dependence of the total intensity resembles the results of band structure calculations⁴⁸. Generally three issues result in poor agreement of theory with experiment: Imperfect surface preparation often leads to disorder, aging of the sample results in surface oxidation, and the discrepancies with calculated spectra may arise from shortcomings of the calculations themselves, e.g. the neglect of surface states. However, calculations of surface states of non-stoichiometric $\text{Co}_2\text{MnSi}(100)$ thin films are available¹⁶, which were used to explain the low spin polarization of about 20% measured by UPS ($h\nu=5.9$ eV) on ex-situ prepared and in-situ sputter cleaned $\text{Co}_2\text{Mn}_{1.19}\text{Si}_{0.88}$ thin films. Fetzer et al.⁴⁹ published experiments of ex-situ prepared stoichiometric $\text{Co}_2\text{MnSi}(100)$ capped by 20 monolayers of MgO through which they obtained spin resolved UPS data ($h\nu=5.9$ eV). They identified no interface states, which they attributed to defects at the $\text{Co}_2\text{MnSi}/\text{MgO}$ interface. A spin polarization of about 40% was obtained. Another way to avoid spurious photoemission results due to degraded sample surfaces is the use of less surface-sensitive hard x-ray photoemission spectroscopy (HAXPES). The identification of several experimentally obtained intensity features with the density of states (DOS) was possible for materials like $\text{NiTi}_{0.9}\text{Sc}_{0.1}\text{Sn}$, NiMnSb or $\text{Co}_x\text{Mn}_y\text{Ge}_z$ ($x : z = 2 : 0.38$) thin Heusler films^{50,51}. However, due to the low intensities of HAXPES experiments no spin resolved results are available up to now. We demonstrated that by in-situ UPS with highly efficient spin-filtering⁵² on epitaxial Heusler thin films the problem of surface degradation can be solved and a spin polarization of 55% investigating Co_2MnGa could be obtained⁵³. Very recently, we measured a record value of 93% at room temperature investigating Co_2MnSi by this method¹⁸.

III. DISCUSSION

In Fig. 1 we present the fully-relativistic band structure calculated for the Δ -direction of the bulk Brillouin zone. The Co_2MnSi -films are magnetized in-plane along the $\bar{\Gamma}-\bar{M}$ line of the surface Brillouin zone. However, we have calculated additionally the bulk-band dispersions for a magnetization direction perpendicular to the sur-

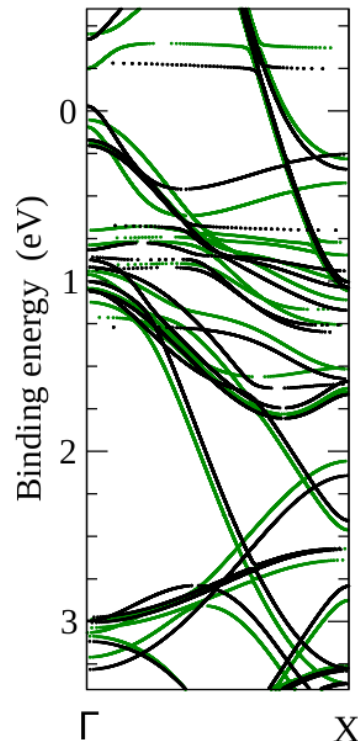


FIG. 1: Relativistic bulk band structure calculated along the Δ -direction for a magnetization direction perpendicular to the (001)-surface (black color) and for an in-plane magnetization direction along $\bar{\Gamma}-\bar{M}$ (green, light color).

face to demonstrate that the dispersion strongly depends on the magnetization direction. This behavior results from the interplay between spin-orbit-coupling (SOC) and magnetic exchange interaction and depends on the band symmetry³⁸. Here, the magnetization direction perpendicular to the surface is indicated by black color and the in-plane direction as given from the experimental conditions is marked by green (light) color. As the underlying symmetry is different for these two cases the spin-orbit coupling causes pronounced changes in the dispersion and energetic position of nearly all bands, if the magnetization is switched from in-plane to out-of-plane direction. The corresponding energy-band splittings and hybridization gaps typically range from some meV up to about 100 meV. In contrast the calculated magnetocrystalline anisotropy energy (MAE), which is defined as the energy difference between $\Delta E_{MAE} = E_{M||[001]} - E_{M||[110]}$ of bulk Co_2MnSi results to $\Delta E_{MAE} = 0.4$ μeV . This should be expected for bulk Co_2MnSi due its cubic structure. The reason for the different energy scales appearing here is found in the fact that the SOC-split energy-band regions only contribute to the MAE if they are located in the vicinity of the Fermi level, where they induce significant deformations of the Fermi surface. As a consequence they do not contribute to the MAE if they appear at finite binding energies. Note that similar effects can be observed for a magnetization which is directed parallel

to the (100) and (001) crystallographic axis. The energetic difference vanishes for the bulk system because these two axis are equivalent. In this case the electronic band structure is invariant under rotations of the quantization axis together with the magnetization direction³⁹. As discussed before, this means that all these modifications cancel each other after integration over all occupied states and do not contribute (as in the cases of (100) and (001) directions) or only create very small contributions (in the present case of (110) and (001) directions) to the magnetocrystalline anisotropy.

One should expect that also surface-related features of the electronic structure will be significantly influenced if the magnetization direction changes. This is indeed the case and will be discussed later in context with the nearly 100% spin polarization which was found for in-plane magnetized samples. Next we inspect the electronic structure of $\text{Co}_2\text{MnSi}(100)$ along the two high symmetry directions $\bar{\Gamma}-\bar{M}$ and $\bar{\Gamma}-\bar{X}$ of the two-dimensional Brillouin zone. The bulk states of Co_2MnSi projected along these two directions are shown in Figs. 2 and 3, where black color indicates bulk-like regions. The left panels present the majority states and the right panels the corresponding minority states, with the total gaps visible in the minority projected bulk-band structures around the Fermi level E_F . Besides the total gaps appearing in the bulk-related minority spin states no further gap structures are visible below E_F . Only for binding energies higher than about 1.5 eV symmetry-induced off-normal gaps exist. As a consequence one would not expect to find pronounced surface-related features dispersing in this binding-energy regime. The situation is different for the unoccupied states. Relatively small gaps appear in both minority spin-projected bulk-band structures just above the Fermi level for nonzero k_{\parallel} values. Furthermore, along $\bar{\Gamma}-\bar{M}$ larger off-normal gaps appear in the majority-spin projected band structure near the \bar{M} point, serving this way as an important precondition

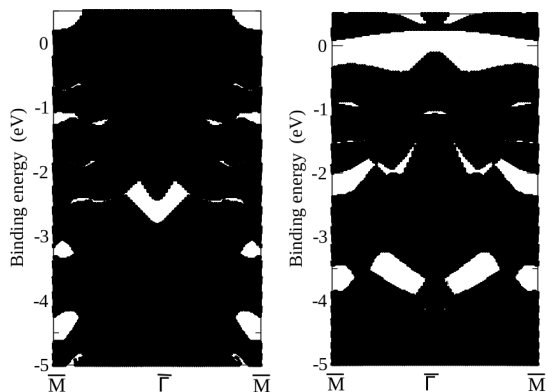


FIG. 2: Projected relativistic bulk band structures for majority spin (left panel) and minority spin character (right panel) along the $\bar{\Gamma}-\bar{M}$ direction. Dark colored regions represent the projection of bulk states.

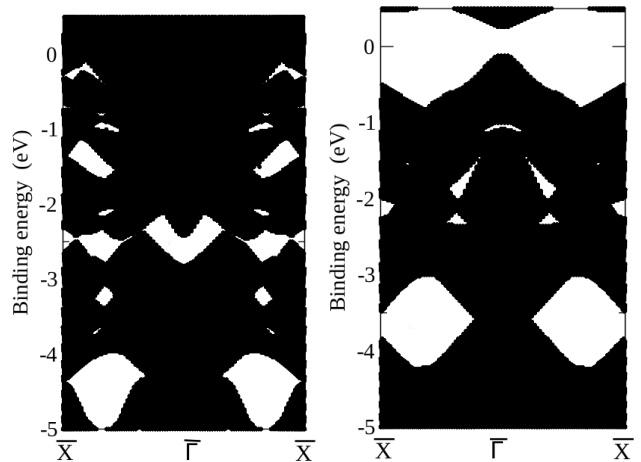


FIG. 3: Projected relativistic bulk band structures for majority spin (left panel) and minority spin character (right panel) along $\bar{\Gamma}-\bar{X}$ direction. Dark colored regions represent the projection of bulk states.

for the existence of surface resonances. The problem with ground state electronic structure calculations is that surface-related features are often hidden in the continuum of bulk states, because of their relatively small spectral weight. Their determination by use of photoemission calculations is often more successful as surface resonances are typically enhanced in their spectral weight due to the excitation process. This is a typical matrix element effect. Furthermore, the determinant criterion⁵⁴ allows for an additional check on the surface contribution of a specific spectral distribution.

In the following angle-integrated photocurrent calculations will be presented for the occupied states (AI-UPS), as well as for the unoccupied states (AI-IPE), where IPE means inverse photoemission. Fig. 4 shows a series of spectra calculated for linear p-polarized light as a function of the photon energy. The incidence angle of the incoming photon beam was chosen $\theta_p=45^\circ$ with respect to the surface normal. Just below the Fermi level a surface-related intensity distribution appears. This signal has to be attributed to the majority surface resonance which is located about 0.4 eV above E_F . Due to convolution with a Fermi distribution function for room temperature and due to a Gauss folding with full width at half maximum of 0.2 eV the tail of this spectral features seems to appear as a peak located at a finite binding energy^{55,56}. At about 1.2 eV binding energy a bulk-like signal is shown which could be attributed to Co and Mn majority d-states. The peak is visible over the whole range of photon energies but with the highest intensity around 20 eV excitation energy. The dispersion is not very pronounced with the tendency that the peak disperses to lower binding energies for higher photon energies. A third spectral feature is found at about 2.5 eV binding energy, also with a less pronounced dispersion and relatively small variations in the maximum intensity. These features also originate

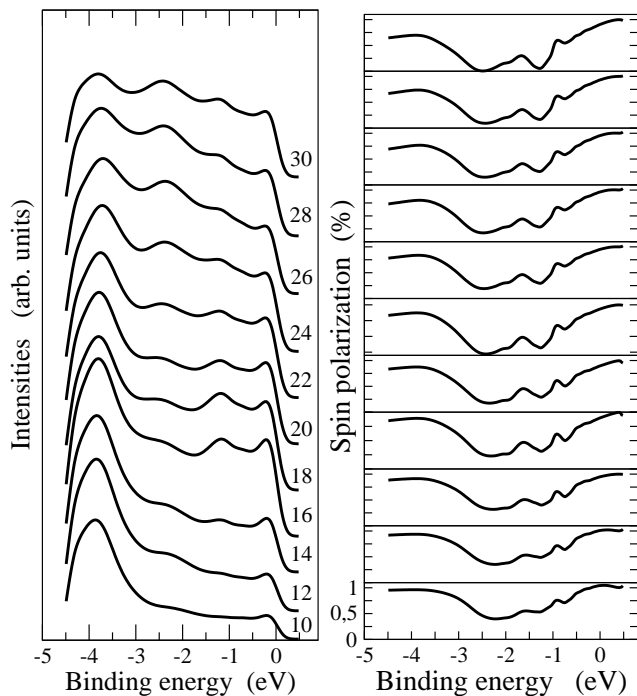


FIG. 4: Left panel: Angle-integrated photoemission spectra calculated for different photon energies in the range from $h\nu = 10$ to 30 eV for p-polarized light. Right panel: In-plane component of the spin polarization vector calculated along $\bar{\Gamma}-\bar{M}$.

from majority Co and Mn-d states. The last spectral feature appears at about 4 eV binding energy and represents excitation from majority Co and Mn d-states, as well as from Si p-states. In the right panel of Fig. 4 we present the corresponding spin polarization as a function of the excitation energy. First, one may observe that for all photon energies the spin polarization reaches nearly 100% in the vicinity of the Fermi level. The spin polarization decreases to about 40% for binding energies around 2 eV. For higher binding energies up to 4.5 eV the spin polarization increases again and reaches high polarization values between 75% and 95%, where the increase is more pronounced for lower excitation energies. This result is in excellent agreement with corresponding experimental data available for photon energies of $h\nu=16.67$ eV and $h\nu=21.2$ eV, and will be discussed in more detail below. As a next step we want to find out the reason for these unexpected high spin-polarization values at the Fermi level. To do so spin-resolved IPE spectra have been calculated, again as a function of the photon energy. The result is presented in Fig. 5, where the left panel shows the intensity distributions and the right panel the corresponding spin polarizations. Two dominant spectral features appear for all excitation energies. The unoccupied majority surface resonance (SR), which is responsible for the spectral intensity just below E_F , and the series of image-potential states which are hidden in the broad peak at about 3.2 eV above E_F . The resonance is very intense

and it is nearly 100% spin-polarized. This is clearly seen in the right panel of Fig. 5, where the spin polarizations are shown. This way our analysis reveals that the pure bulk contribution of the experimental spin polarization, which due to the limited experimental energy resolution was about 50% only, is increased to about 100% by the surface resonance.

Even more, the amount of spectral weight and the high spin polarization value of this spectral feature are intimately connected with the in-plane magnetization of the sample. In case where the magnetization is directed perpendicular to the surface this resonance vanishes with a very low spectral weight into the bulk continuum, and instead one observes an occupied minority surface state located just below E_F . As a consequence the spin polarization at the Fermi level is reduced to values significantly smaller than the pure bulk value. The origin for this peculiar behavior is found in the very different electronic structures, which result for in-plane and out-of-plane magnetization directions of the sample surface. This is clearly seen, if one inspects Fig. 1 again.

In Fig. 6 the spectroscopical calculations and the experimental spin-integrated UPS and HAXPES results are compared. Nearly quantitative agreement for both, UV and hard X-ray photon energies, is obtained. Only the intensity distribution calculated just below E_F at $h\nu=16.67$ eV is overestimated in comparison with the experimental data. The reason is found in the energy-dependent

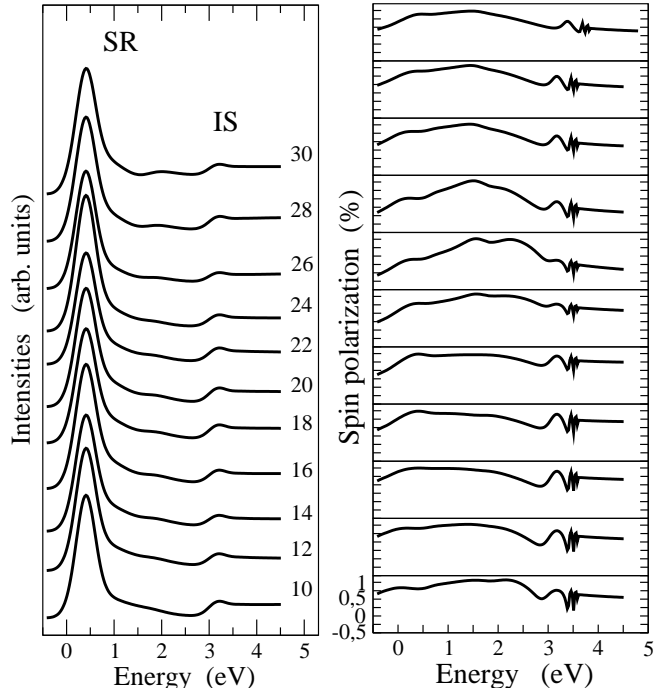


FIG. 5: Left panel: Angle-integrated inverse photoemission spectra calculated for different photon energies in the range from $h\nu = 10$ to 30 eV for p-polarized light. Right panel: In-plane component of the spin polarization vector calculated along $\bar{\Gamma}-\bar{M}$.

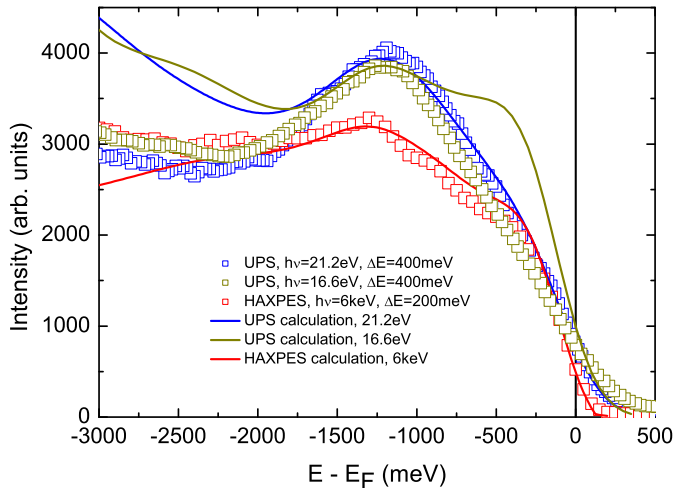


FIG. 6: Comparison of measured and calculated AI-UPS and angle-integrated HAXPES spectra. The HAXPES data have been collected from ex situ capped Co_2MnSi thin layers with an energy resolution of $\Delta E=200$ meV for a photon energy of $h\nu=6$ keV. The AI-UPS spectra were measured in situ on an uncapped Co_2MnSi layer with an energy resolution of $\Delta E=400$ meV for two different photon energies of $h\nu=16.67$ and 21.2 eV. The corresponding one-step photoemission calculations are based on electronic structure calculations in the framework of the SPRKKR+DMFT method with U-parameters $U_{\text{Mn}}=3.0$ eV and $U_{\text{Co}}=1.5$ eV for Mn and Co.

cross section of the surface resonance which increases at lower photon energies because of the energy-dependent multiple scattering between bulk and surface. As a consequence the wave function of the resonance is strongly energy-dependent and so the corresponding matrix elements. Therefore, the theoretically overestimated spectral distribution may be ascribed to a typical matrix-element effect. Besides this, and with regard to the small DOS just below the Fermi energy the agreement of the calculations with the high UPS and HAXPES intensities in this energy range is remarkably good and it is mostly traced back to this bulk-like surface resonance occurring in the majority-spin channel. The energetic position and dispersion behavior of this spectroscopical feature has been discussed in detail above. Here it remains to remind to the fact that our self-consistent electronic structure calculation leads to a half-metallic band structure with a total gap located around E_F in the minority spin-projected states. But also from our experimental data strong evidence for half-metallicity is provided as we have estimated the position of the lower band edge of the minority gap at about $E-E_F = -0.5$ eV, directly from the corresponding spectroscopical data. As shown in Fig. 6, the inclusion of the complete surface-related photoexcitation in the UPS calculation results in nearly

perfect agreement with experiment. If the surface resonance were not present, half-metallic behavior would persist, but the finite experimental resolution in photoemission would hinder the observation of a high spin polarization. As mentioned before, the theoretical analysis reveals an experimental resolution limited spin polarization lower than 50% for a pure bulk-like calculation. This provides further evidence for the calculated half-metallic band structure of Co_2MnSi .

In Fig. 7 the highest experimentally observed spin polarization is shown together with the calculated spin polarization for two different photon energies of $h\nu=16.67$ and 21.2 eV, and with the corresponding theoretical DOS. The calculated photoemission asymmetries include all relevant broadening effects occurring in the measurements. In particular, the influence of intrinsic life-time broadening generated by electronic correlations, broadening effects from impurity scattering and the experimental resolution of about $\Delta E=0.4$ eV are considered. If one compares first the pure bulk-like theoretical spectrum with the calculated DOS the correspondence between these two intensity distributions is obvious. The broadening effects in combination with the absence of surface-like emission reduce the effective spin polarization tremendously, although half-metallic behavior persists. Considering surface-related effects changes the situation dramatically. A true surface state which typically disperses in a huge gap of a projected bulk-band structure

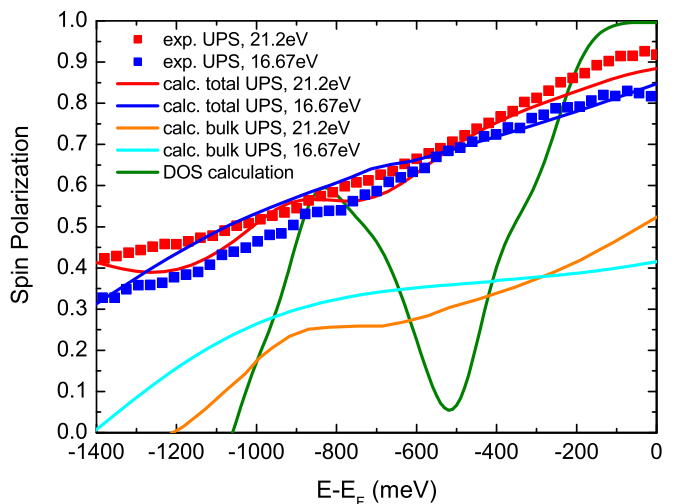


FIG. 7: Comparison of measured spin polarizations, taken in situ from an uncapped Co_2MnSi layer, with calculated ones. Shown are the corresponding results for photon energies of $h\nu=16.67$ and 21.2 eV. In addition a bulk-like calculation of the spin polarization is presented, where the surface contribution of the theoretically obtained photocurrent is suppressed. The calculated DOS is shown in green (light) color, respectively. Data for $h\nu=21.2$ taken from¹⁸.

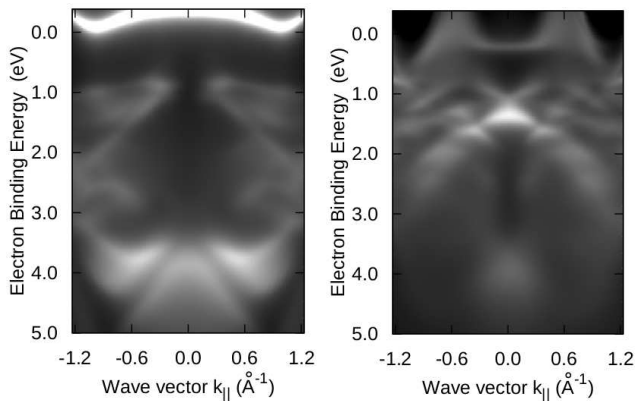


FIG. 8: Contour plots for majority (left panel) and minority (right panel) angle-resolved spectral densities are shown, which have been calculated within the fully relativistic one-step model along the $\bar{\Gamma}$ - \bar{M} direction for a photon energy of $h\nu=21.2$ eV. High spectral weight is indicated by light colors.

shows up with a maximum spectral weight at the first atomic layer. A well known example for such a surface feature is the Shockley state dispersing on the Cu(111)-surface⁵⁷. Therefore, the spectral weight compared to normal bulk states is small. Thus the combined effect of a very short inelastic mean free path and an energy-dependent cross section reduces the spectral weight in the photoemission process significantly. The situation is very different for Co₂MnSi because the majority surface resonance is embedded in the unoccupied bulk continuum with a strong coupling to the majority bulk states. This is because a layer-dependent analysis of the spectral weight showed that the resonance extends over the first six atomic layers of the semi-infinite bulk. This is similar to the case of W(110), where we found a surface resonance revealing a considerable bulk contribution⁵⁸ as well. The spectral weight of this surface resonance is much larger than that of a true surface state resulting in a significant contribution to the total intensity even at hard X-ray energies.

As a last point in our analysis we present spin-resolved ARPES spectra calculated as a function of binding energy and k_{\parallel} -value along the $\bar{\Gamma}$ - \bar{M} direction of the surface Brillouin zone. The left panel of Fig. 8 shows the majority-spin intensity distribution in form of a contour plot. In the right panel the corresponding contour plot for minority-spin states is shown. High spectral weight is indicated by light colors. Not surprisingly, the highest spectral weight belongs to the surface resonance. This is clearly observable from the majority contour plot. This feature slightly disperses around $\bar{\Gamma}$ at about 0.3 eV above the Fermi level. Noticeable is here that this feature disperses towards the Fermi level for higher k_{\parallel} -values and nearly touches E_F at $k_{\parallel} \approx 1.0$ inverse Angström. This result is not obtainable from angle-integrated photocurrent calculations. It supports even more our finding that the resonance is able to enhance the experimental resolution

limited spin polarization by almost a factor of two, although this feature seems to be located quite far from the Fermi level if only calculated AI-UPS data are inspected. At about 0.5 eV binding energy the bulk states show up to disperse as a function of E and k_{\parallel} . At lower binding energies in the region between 0.5 and 3 eV mainly Co and Mn majority d-states are visible, where at higher binding energies around 4 eV a mixture of Si p-states and Co and Mn d-states exists with stronger dispersion behavior. In agreement with our DOS calculations the spectral features dispersing down to about 5 eV are more intense in their spectral signals than most of the states at lower binding energies. This is due to the intense peak appearing in the DOS, which is ascribed to Si p-states, and is obviously a shortcoming of the electronic structure calculation as discussed in detail in Ref. 15.

In the right panel of Fig. 8 we present the minority states in form of an E versus k_{\parallel} contour plot. Besides the fact that the minority Mn and Co d-states are visible with their dispersion in k_{\parallel} , the most interesting observation is the non-vanishing spectral density at the Fermi level. At k_{\parallel} -values of about ± 0.6 inverse Angström a nonzero spectral signal is present. This is the fingerprint of a minority surface state which disperses into the total gap of the minority spin-projected bulk-band structure. This feature is not visible in the AI-UPS spectra because of its low spectral weight. The origin for this peculiar result is found in the in-plane magnetization of the sample. In fact this true surface state appears with high spectral weight if the magnetization of the corresponding sample points perpendicular to the surface, where the spectral weight of our surface resonance decreases strongly. The existence of this feature, even for a 100% in-plane magnetized sample surface is the most possible reason why the spin polarization is reduced by a few percent from 100% to about 93%.

IV. SUMMARY

In conclusion, we were able to demonstrate half-metallic behavior for Co₂MnSi in combination with a nearly 100% spin polarization at room temperature, directly measured and confirmed by our theoretical analysis. Our spectroscopical work has clearly demonstrated that the spin polarization very sensitively depends on the interplay of bulk- and surface-related spectral features, where the magnetization direction of the sample surface plays a major role. In particular, we found that the high spin polarization at the Fermi energy is related to a stable surface resonance in the majority-spin projected states extending deep into the bulk of the sample. A description within the LSDA approach in combination with the DMFT method results in a quantitative description of the electronic structure of Co₂MnSi. The use of a DMFT+LSDA electronic structure calculation is important, whereas the application of the fully relativistic one-step model of photoemission in its spin-density

matrix formulation guarantees a quantitative analysis of the spectroscopical data. Our observations may serve as a useful information for future spintronic applications on the basis of Heusler alloys.

Acknowledgments

Financial support by the Deutsche Forschungsgemeinschaft through the SFB 925 (project B5), FOR1464 "AS-

PIMATT" (Project P 1.2-A), FOR 1346, Eb-154/23, Eb-154/26 and GSC 266 MAINZ as well as the EU (ERC-2007-StG 208162), is gratefully acknowledged. JM would like to acknowledge the CENTEM project (reg. no. CZ.1.05/2.1.00/03.0088) and CENTEM PLUS (LO1402) cofunded by Ministry of Education, Youth and Sports of Czech Republic.

-
- ¹ D. Hsieh et al., Nature **460**, 1101, (2009).
² A. Takayama et al. Phys. Rev. Lett. **106**, 166401 (2011).
³ K. Miyamoto et al., Phys. Rev. Lett. **108**, 066808 (2012).
⁴ K. P. Kämper, W. Schmitt, and G. Güntherodt, Phys. Rev. Lett. **59**, 2788 (1987).
⁵ S. Yu. et al. Phys. Rev. B **65**, 064417 (2002).
⁶ T. Graf, C. Felser, and S. S. P. Parkin, Prog. Sol. State Chem. **39**, 1 (2011).
⁷ R. A. de Groot, F. M. Mueller, P. G. van Engen, and K. H. J. Bushow, Phys. Rev. Lett. **50**, 2024 (1983).
⁸ S. Plogmann, T. Schlathölter, J. Braun, M. Neumann, Yu. M. Yarmoshenko, M. V. Yablonskikh, E. I. Shreder, E. Z. Kurmaev, A. Wrona, and A. Slebarski, Phys. Rev. B **60**, 6428 (1999).
⁹ H. Kolev, G. Rangelov, J. Braun, and M. Donath, Reduced surface magnetization of NiMnSb(001), Phys. Rev. B **72**, 104415 (2005).
¹⁰ M. Donath, G. Rangelov, J. Braun, and W. Grentz, Magnetization, Spin polarization, and electronic structure of NiMnSb surfaces, in Local-Moment Ferromagnets edited by M. Donath and W. Nolting, Lecture Notes in Physics 678, Springer Verlag (2005).
¹¹ J. S. Correa, Ch. Eibl, G. Rangelov, J. Braun, and M. Donath, Phys. Rev. B **73**, 125316 (2006).
¹² M. V. Yablonskikh, J. Braun, M. T. Kuchel, A. V. Postnikov, M. Neumann, J. D. Denlinger, and A. Moewes, Phys. Rev. B **74**, 085103 (2006).
¹³ J. Minár, J. Braun, S. Bornemann, H. Ebert, and M. Donath, J. Phys. D: Appl. Phys. **42**, 084009 (2009).
¹⁴ M. I. Katsnelson et al. Rev. Mod. Phys. **80**, 315 (2008).
¹⁵ S. Chadov, G. H. Fecher, C. Felser, J. Minár, J. Braun, and H. Ebert, J. Phys. D: Appl. Phys. **42**, 084002 (2009).
¹⁶ J. P. Wüstenberg, M. Aeschlimann, M. Cinchetti, J. Minár, J. Braun, H. Ebert, T. Ishikawa, and M. Yamamoto, Co₂MnSi, Phys. Rev. B **85**, 064407 (2012).
¹⁷ J. Braun, H. Ebert and J. Minár, Correlation and chemical disorder in Heusler alloys: A spectroscopical study, in Spintronics; From Materials to Devices, Editors C. Felser and G. H. Fecher, 97, Springer (2013).
¹⁸ M. Jourdan et al., Nat. Commun. **5**, 3974 (2014).
¹⁹ B. Feuerbacher, B. Fitton, and R. F. Willis, editors, *Photoemission and the Electronic Properties of Surfaces*, (Wiley, New York, 1978); M. Cardona and L. Ley, editors, *Photoemission in Solids* volume 1, (Springer, Berlin, 1978); J. E. Inglesfield, Rep. Prog. Phys. **45**, 223 (1982);
²⁰ V. Dose, Prog. Surf. Sci. **13**, 225 (1983); Surf. Sci. Rep. **5**, 337 (1985); G. Borstel and G. Thörner, Surf. Sci. Rep. **8**, 1 (1988); N. V. Smith, Rep. Prog. Phys. **51**, 1227 (1988);
M. Donath, Surf. Sci. Rep. **20**, 251 (1994).
²¹ J. B. Pendry, Low Energy Electron Diffraction (Academic, London, 1974).
²² J. B. Pendry, Surf. Sci. **57**, 679 (1976).
²³ J. F. L. Hopkinson, J. B. Pendry, and D. J. Titterton, Comput. Phys. Commun. **19**, 69 (1980).
²⁴ B. Ginatempo, P. J. Durham, and B. I. Gyorffy, J. Phys. C **1**, 6483 (1983); S. V. Halilov, E. Tamura, H. Gollisch, D. Meinert, and R. Feder, J. Phys.: Condens. Matter **5**, 3859 (1993); J. Henk, S. V. Halilov, T. Scheunemann, and R. Feder, Phys. Rev. B **50**, 8130 (1994); M. Fluchtmann, M. Graß, J. Braun, and G. Borstel, Phys. Rev. B **95**, 9564 (1995).
²⁵ J. Braun, Rep. Prog. Phys. **59**, 1267 (1996).
²⁶ S. V. Halilov, E. Tamura, D. Meinert, H. Gollisch, and R. Feder J. Phys. Condens. Matter **5**, 3859 (1993).
²⁷ G. Borstel, Appl. Phys. A **38**, 193 (1985).
²⁸ C. Caroli, D. Lederer-Rozenblatt, B. Roulet, and D. Saint-James, Phys. Rev. B **8**, 4552 (1973).
²⁹ J. Braun, New developments in UPS and XPS from ferromagnetic materials, in Band-Ferromagnetism: Ground-State and Finite-Temperature Phenomena, editors K. Baberschke, M. Donath and W. Nolting, vol 580, from Lecture Notes in Physics, 267 (Springer, Berlin, 2001).
³⁰ G. Hilgers, M. Potthoff, N. Müller, U. Heinzmann, L. Haunert, J. Braun, and G. Borstel, Phys. Rev. B **52**, 14859 (1995).
³¹ J. P. Perdew, K. Burke, and M. Ernzerhof, Phys. Rev. Lett. **77**, 3865 (1996).
³² J. Minár J. Phys.: Cond. Mat. **23**, 253201 (2011).
³³ J. Minár, L. Chioncel, A. Perlov, H. Ebert, M. I. Katsnelson, and A. I. Lichtenstein, Phys. Rev. B **72**, 045125 (2005).
³⁴ H. Ebert, D. Ködderitzsch and J. Minár, Rep. Prog. Phys. **74**, 096501 (2012).
³⁵ H. Ebert et al., The munich SPR-KKR package, version 7.2, <http://olymp.cup.uni-muenchen.de/~ak/ebert/SPRKKR> (2012).
³⁶ L. V. Pourovskii, M. I. Katsnelson and A. I. Lichtenstein, Phys. Rev. B **72**, 115106 (2005).
³⁷ M. Meinert, C. Friedrich, G. Reiss and S. Blügel, Phys. Rev. B **86**, 245115 (2012).
³⁸ G. H. O. Daalderop, P. J. Kelly, and M. F. H. Schuurmans, Phys. Rev. B **50**, 9989 (1994).
³⁹ J. Stöhr, Journal of Magnetism and Magnetic Materials **200**, 470 (1999).
⁴⁰ S. Ouazi, S. Vlaic, S. Rusponi, G. Moulas, P. Buluscek, K. Halleux, S. Bornemann, S. Mankovsky, J. Minar, J.B.

- Staunton, H. Ebert and H. Brune Nat. Commun. **3**, 1313 (2012).
- ⁴¹ S. Bornemann, PhD thesis, LMU Munich (2011), <http://edoc.ub.uni-muenchen.de/14207/>
- ⁴² G. Malmström and J. Rundgren, Comput. Phys. Commun. **19**, 263 (1980).
- ⁴³ A. Nuber, J. Braun, F. Forster, J. Minár, F. Reinert, and H. Ebert, Phys. Rev. B **83**, 165401 (2011).
- ⁴⁴ A. Bendounan, K. Ait-Mansour, J. Braun, J. Minár, S. Bornemann, R. Fasel, O. Gröning, F. Sirotti, and H. Ebert, Phys. Rev. B **83**, 195427 (2011).
- ⁴⁵ J. F. L. Hopkinson, J. B. Pendry, and D. J. Titterton, Comput. Phys. Commun. **19**, 69 (1980).
- ⁴⁶ W. H. Wang et al. Phys. Rev. B **71**, 144416 (2005).
- ⁴⁷ Feng Wu et al. Appl. Phys. Lett. **94**, 122503 (2009).
- ⁴⁸ S. Wurmehl et al., J. Phys. D: Appl. Phys. **39**, 803 (2006).
- ⁴⁹ R. Fetzter et al. Phys. Rev B, **87**, 184418 (2013).
- ⁵⁰ S. Ouardi et al., Phys. Rev. Lett. **107**, 036402 (2011).
- ⁵¹ S. Ouardi et al. Appl. Phys. A **111**, 395 (2013).
- ⁵² M. Kolbe et al. Phys. Rev. Lett. **107**, 207601 (2011).
- ⁵³ M. Kolbe et al. Phys. Rev. B **86**, 024422 (2012).
- ⁵⁴ J. Braun and M. Donath, J. Phys. Condens. Mat. **16**, S2539 (2004).
- ⁵⁵ M. Donath and V. Dose, Euro. Phys. Lett. **9**, 821 (1989)
- ⁵⁶ S. D. Stolwijk, A. B. Schmidt and M. Donath, Phys. Rev. B **82**, 201412(R) (2010).
- ⁵⁷ M. Grass, J. Braun, G. Borstel, R. Schneider, H. Dürr, Th. Fauster, and V. Dose, J. Phys. Condens. Matter **5**, 599 (1993).
- ⁵⁸ J. Braun et al. New J. Phys. **16**, 015005 (2014).